Performance Evaluation Statistics Applied to Derived Fields of NWP Model Forecasts

PRAKKI SATYAMURTY AND DANIEL PIRES BITTENCOURT

Centro de Previsão de Tempo e Estudos Climáticos, Instituto Nacional de Pesquisas Espaciais, Cachoeira Paulista, Sao Paulo, Brazil

(Manuscript received 5 May 1998, in final form 12 April 1999)

ABSTRACT

NWP model skill as obtained from the standard statistics applied to derived atmospheric fields such as thermal advection and moisture convergence is different from that obtained by the same statistics applied to basic model output fields such as temperature or wind components. An analysis with a combination of two simple wave functions shows that the errors in the forecast of the phase of the shortwave component are overwhelmingly more important. For an error of 2° longitude in the phase forecast of the shortwave component (wavenumber ~20) the correlation coefficient for the derived fields is only 0.7 whereas it is nearly 0.9 for the basic variable fields. The prediction range of useful forecasts in terms of the derived variables decreases drastically in comparison to that obtained with the simple variables. These aspects are demonstrated with the Centro de Previsão de Tempo e Estudos Climáticos–Center for Ocean–Land–Atmosphere studies operational NWP model in two real synoptic cases that are representative of active weather situations in austral winter over the southern half of South America.

1. Introduction

In model performance evaluations (Chen and Van den Dool 1995; Wilks 1995) it is customary to use the spatial linear correlation $r(F, A)$ between the anomaly of the forecast field, F, valid for time t and the anomaly of the verifying analysis field, A, for the same instant over a sufficiently large region of a horizontal or isobaric surface. This parameter measures the spatial similarity between the forecast and the verifying fields over and above the climatology for the region. The expression for the statistical parameter is

$$r(F, A) = \frac{1}{N} \sum_i (F_i' A_i')/(\sigma_F \sigma_A), \tag{1}$$

where σ_F and σ_A are the spatial standard deviations of F and A, respectively; the suffix i indicates the ith grid point; the prime indicates the deviation from the spatial mean after subtracting the climatology; and the summation, Σ_i, is from $i = 1$ to N in which N is the total number of grid points over the region. If the grid over the region considered is formed by k points in the x direction and l points in the y direction, then $N = kl$.

In addition, root-mean-square error $E(F, A)$ of F with respect to A is employed to quantify the forecast error. The expression is

$$E(F, A) = \frac{1}{N} \left[\sum_i (F_i - A_i)^2 \right]^{1/2}. \tag{2}$$

Parameters r and E indicate the reliability of the forecast over the region.

The general criteria used to consider a forecast field as useful are

$$\begin{aligned} &\text{(i)} && \sigma_F \approx \sigma_A \\ &\text{(ii)} && E(F, A) \leq \sigma_A \\ &\text{(iii)} && r(F, A) \geq 0.6. \end{aligned} \tag{3}$$

These statistics and criteria are normally applied to the standard basic model output variables: the sea level pressure p_s, 500-hPa geopotential height ϕ_{500}, 850-hPa wind $\mathbf{V}_{850}$, 250-hPa wind $\mathbf{V}_{250}$, and 1000-hPa virtual temperature $T_{\mathbf{V}_{1000}}$. Model intercomparisons and studies of temporal variations in the performance of numerical weather prediction (NWP) models are accomplished through these statistics (Wobus and Kalnay 1995).

However, atmospheric variables such as the thermal advection, the vorticity advection, and the humidity flux convergence display the essence of a given synoptic situation, and therefore a comparison of their forecast and observed verification fields is interesting and reveals the model performance in terms of the dynamical processes they describe. The question addressed in the present paper is whether the performance obtained through the basic variables (such as $T_{\mathbf{V}_{850}}$) of the model and the perfomance obtained through the derived variables (such as thermal advection) are essentially similar or are different. A simple analysis with hypothetical si-

Corresponding author address: Dr. Prakki Satyamurty, CPTEC-INPE, Rodovia Presidente Dutra-Km 40, Cachoeira Paulista, SP, CEP 12.630-000, Brazil.
E-mail: saty@cptec.inpe.br

nusoidal fields is performed to show possible differences in the anomaly correlations of the basic and derived meteorological variables. These differences are presented with the aid of two real synoptic cases that are representative of the active weather situations over the southern half of South America.

2. Analysis with simple wave functions

Considering a one-dimensional basic meteorological variable in longitude (λ), for simplicity, we let the verification and forecast fields to be a combination of two wavenumbers m and n such that

$$A = a_m \sin m\lambda + a_n \sin n\lambda \quad \text{and}$$

$$F = b_m \sin m(\lambda + \epsilon_m) + b_n \sin n(\lambda + \epsilon_n), \quad (4)$$

where a_m, a_n and b_m, b_n are the amplitudes of the verification and forecast fields, respectively, and ϵ_m, ϵ_n are the phase differences between the forecast and the verification fields for the harmonics m and n. The correlation between F and A is calculated to be

$$r(F, A) = [(a_m b_m \cos m\epsilon_m + a_n b_n \cos n\epsilon_n)] \div [(a_m^2 + a_n^2)^{1/2}(b_m^2 + b_n^2)^{1/2}]. \quad (5)$$

Now considering the derivatives F_λ and A_λ of the forecast and verification fields with respect to λ, their correlation is calculated to be

$$r(F_\lambda, A_\lambda) = [(m^2 a_m b_m \cos m\epsilon_m + n^2 a_n b_n \cos n\epsilon_n)] \div [(m^2 a_m^2 + n^2 a_n^2)^{1/2}(m^2 b_m^2 + n^2 b_n^2)^{1/2}]. \quad (6)$$

Although the expressions in Eqs. (5) and (6) are both highly dependent on the phase angles, clearly they are different. Even in the simpler case where, say, $a_m = a_n = b_m = b_n = 1$, the expressions are

$$r(F, A) = (\cos m\epsilon_m + \cos n\epsilon_n)/2 \quad (7)$$

$$r(F_\lambda, A_\lambda) = (m^2 \cos m\epsilon_m + n^2 \cos n\epsilon_n)/(m^2 + n^2). \quad (8)$$

Depending on the relative magnitudes of m and n the numerical value of r in the two expressions in Eqs. (7) and (8) can differ substantially. To further appreciate this difference let us consider an example where $n = 2m$. Then the two expressions take the following forms:

$$r(F, A) = (\cos m\epsilon_m + \cos 2m\epsilon_n)/2 \quad (9)$$

$$r(F_\lambda, A_\lambda) = (\cos m\epsilon_m + 4 \cos 2m\epsilon_n)/5. \quad (10)$$

From the above it is quite evident that the phase of the larger wavenumber (or smaller wavelength) is far more important than that of the smaller wavenumber (or longer wavelength) in determining the correlation between the derived fields F_λ and A_λ. The correlation between the forecast and verification derived fields can be substantially different from that between the basic variable forecast and its verification. The quality of the forecast of shorter waves is more important when the derived variables are considered in the evaluation of model performance.

The differences between Eqs. (5) and (6) above are demonstrated in Figs. 1–4. For $a_m = a_n = b_m = b_n = 1$ and for the phase differences $\epsilon_m = \epsilon_n = 2°$ the correlations $r(F, A)$ and $r(F_\lambda, A_\lambda)$ between the forecast fields and the corresponding verification fields in the wavenumber domain $m, n = 0, 1, 2, \ldots, 20$ are presented in Figs. 1a and 1b. It is clear that $r(F, A)$ (Fig. 1a) is different from $r(F_\lambda, A_\lambda)$ (Fig. 1b) for higher wavenumbers where the anomaly correlation between the derived fields is less than the correlation between the basic fields. These differences become larger for larger phase differences as shown in Figs. 1c and 1d for $\epsilon_m = \epsilon_n = 5°$ and in Figs. 1e and 1f for $\epsilon_m = \epsilon_n = 7°$.

Results for the cases in which one of the harmonics is forecast with no phase difference ($\epsilon_n = 0$) and the other with phase differences of $\epsilon_m = 2°$, 5°, and 7° are presented in Fig. 2. Figures 2a and 2b show that for a combination of a short wave, say, $n = 20$ and a synoptic wave, say, $m = 8$, and a 2° phase error in the forecast field of the short wave, the anomaly correlation is approximately 0.9 for the basic fields and is 0.7 for the derived fields. It can be verified from Figs. 2e and 2f that at around m (on the abscissa) = 13; that is, when the phase difference between the forecast field and the verification field is such that $m\epsilon_m$ is $\pi/2$, $r(F, A)$ becomes 0.5 independent of n whereas Fig. 2f shows that $r(F_\lambda, A_\lambda)$ is far less than 0.5 even for small n and becomes still smaller for large n. Note from Eq. (6) that in $r(F_\lambda, A_\lambda)$ the term in n^2 dominates for large n and the term in m^2 dominates for large m whereas in $r(F, A)$ [Eq. (5)] there is no such dependence. These differences between the correlations of basic fields and the correlations of the derived fields are larger for larger phase differences and the correlation can even become negative for the derived fields.

Figures 3a to 3f show comparisons between the values of $r(F, A)$ and $r(F_\lambda, A_\lambda)$ for some combinations of ϵ_m and ϵ_n. The skewness of the correlation values with respect m and n when $\epsilon_m \neq \epsilon_n$ is evident, but in general $r(F_\lambda, A_\lambda)$ is smaller than $r(F, A)$, especially for large m or n and for large phase errors between the forecast and its verification. Figures 4a to 4f show the differences between $r(F, A)$ and $r(F_\lambda, A_\lambda)$ for a few cases in which the amplitudes of the component waves are different.

3. Description of NWP model and its performance

The Centro de Previsão de Tempo e Estudos Climáticos (CPTEC) Center for Ocean–Land–Atmosphere Studies (COLA) global spectral atmospheric general circulation model with an approximate horizontal resolution of 200 km (T62 L28) is employed for operational numerical weather prediction (NWP) at CPTEC in Brazil. This model has the following physics. It has the modified-Kuo deep convection parameterization described by Sela (1980) and the shallow convection

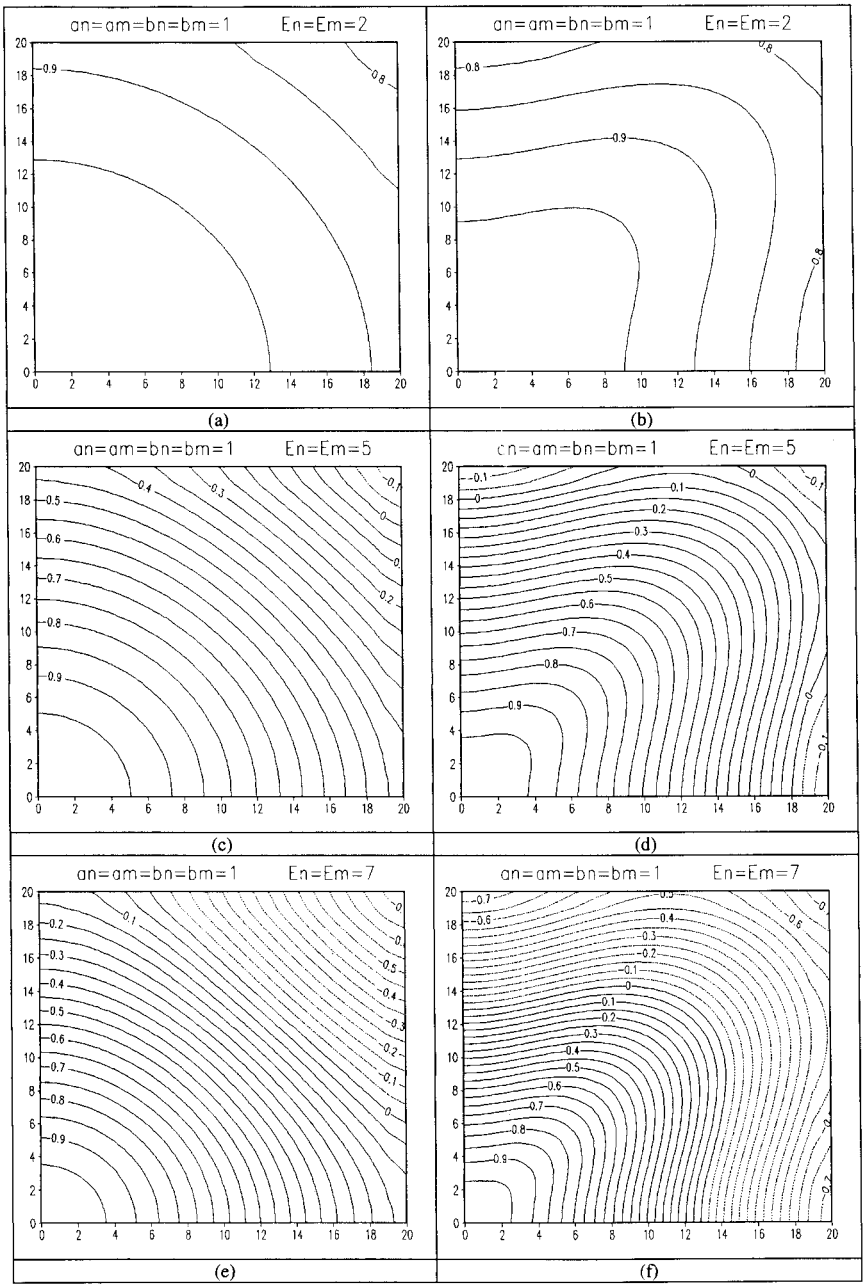

FIG. 1. Anomaly correlation coefficients between the forecast and the verification for basic fields (left panels) and for derived fields (right panels) for the case of $a_m = a_n = b_m = b_n = 1$ and $\epsilon_m = \epsilon_n \neq 0$ in the wavenumber domain. Abscissa represents wavenumber n and the ordinate wavenumber m: (a) $r(F, A)$ for $\epsilon_m = \epsilon_n = 2°$, (b) $r(F_\lambda, A_\lambda)$ for $\epsilon_m = \epsilon_n = 2°$, (c) $r(F, A)$ for $\epsilon_m = \epsilon_n = 5°$, (d) $r(F_\lambda, A_\lambda)$ for $\epsilon_m = \epsilon_n = 5°$, (e) $r(F, A)$ for $\epsilon_m = \epsilon_n = 7°$, (f) $r(F_\lambda, A_\lambda)$ for $\epsilon_m = \epsilon_n = 7°$.

scheme of Tiedtke (1983) in addition to large-scale precipitation. Longwave radiation (Harshvardhan et al. 1987) including the iterative cloud radiation scheme of Slingo (1987) is calculated every 3 h of simulation and the shortwave radiation (Lacis and Hansen 1974) is calculated every 1 h of simulation. The model also contains (i) the simple biosphere model of Sellers et al. (1986) as formulated by Xue et al. (1991) over the land and the bulk aerodynamic scheme of Miyakoda and Sirutis (1986) over the oceans, (ii) the planetary boundary layer scheme of Mellor and Yamada (1982), and (iii) the gravity wave drag scheme of Kirtman et al. (1993).

The operational performance of the CPTEC–COLA model is evaluated using the standard basic variables

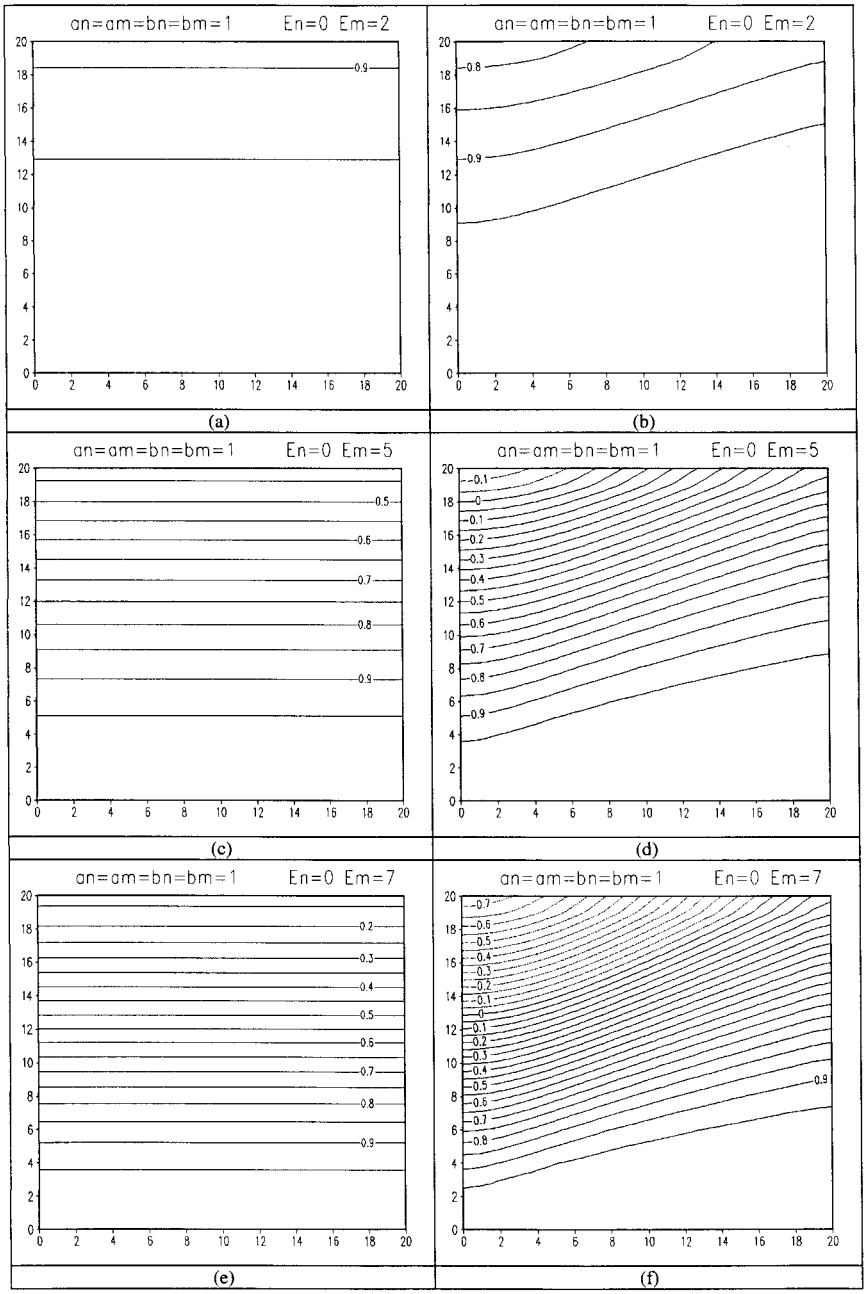

FIG. 2. Same as in Fig. 1 except for $\epsilon_n = 0$ and $\epsilon_m \neq 0$: (a) $r(F, A)$ for $\epsilon_m = 2°$, (b) $r(F_\lambda, A_\lambda)$ for $\epsilon_m = 2°$, (c) $r(F, A)$ for $\epsilon_m = 5°$, (d) $r(F_\lambda, A_\lambda)$ for $\epsilon_m = 5°$, (e) $r(F, A)$ for $\epsilon_m = 7°$, (f) $r(F_\lambda, A_\lambda)$ for $\epsilon_m = 7°$.

and the standard statistics mentioned above as is the case with all the operational NWP models worldwide (Stanski et al. 1990). According to Bonatti (1996) the 500-hPa geopotential anomaly correlation skill of the CPTEC–COLA model is higher than 60% at day 5 of the forecasts for the South American region (15°–60°S, 90°–20°W). In terms of 850-hPa virtual temperature the skill decreases from higher than 60% at day 4 to slightly lower than 60% at day 5. These skill scores are better in austral winter than in austral summer.

In the present study the derived variables used for model evaluation are the divergence ($D = \nabla \cdot \mathbf{V}$) at the 850-hPa level; the convergence of water vapor flux ($\nabla \cdot q\mathbf{V}$) at the 850-hPa level; the thermal advection ($\mathbf{V} \cdot \nabla T_v$) at the 850-hPa level; the vorticity, ζ, at the 500- and 200-hPa levels; and the vorticity advection

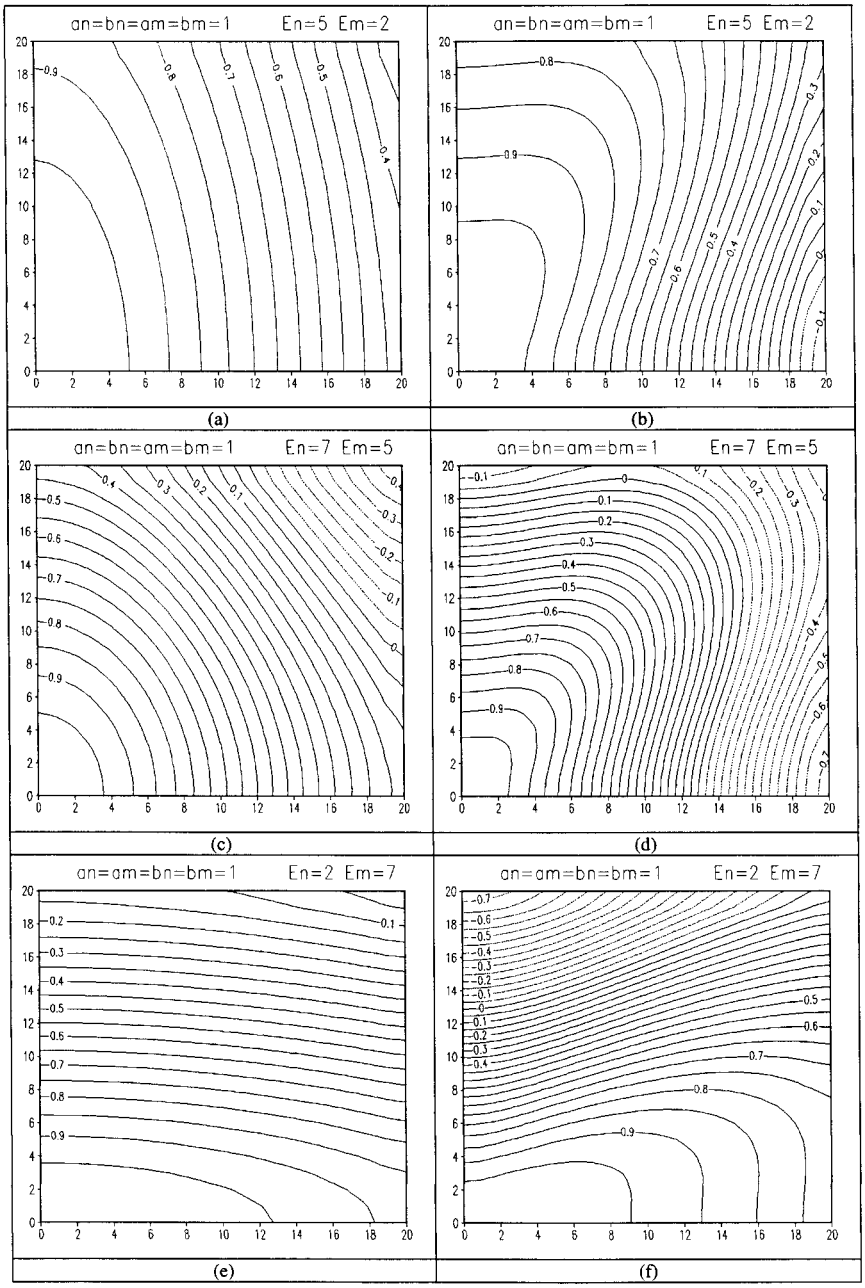

FIG. 3. Same as in Fig. 1 except for $\epsilon_m \neq \epsilon_n$: (a) $r(F, A)$ for $\epsilon_m = 2°$, $\epsilon_n = 5°$, (b) $r(F_\lambda, A_\lambda)$ for $\epsilon_m = 2°$, $\epsilon_n = 5°$, (c) $r(F, A)$ for $\epsilon_m = 5°$, $\epsilon_n = 7°$, (d) $r(F_\lambda, A_\lambda)$ for $\epsilon_m = 5°$, $\epsilon_n = 7°$, (e) $r(F, A)$ for $\epsilon_m = 7°$, $\epsilon_n = 2°$, (f) $r(F_\lambda, A_\lambda)$ for $\epsilon_m = 7°$, $\epsilon_n = 2°$.

$(\mathbf{V} \cdot \nabla\zeta)$ at the 500- and 200-hPa levels. The basic atmospheric variables are the u and v components of wind at the 850-, 500-, and 200-hPa levels and the virtual temperature and specific humidity at 850 hPa. (The symbols used here have the usual meaning.) All these are scalar fields and all the statistics are obtained over the limited region bounded by 15°–60°S, 90°–20°W containing all the extratropical area of the South American continent. The 15-yr climatology for the period 1979–93 from the U.S. National Centers for Environmental Prediction is used for obtaining the anomalies for the domain considered.

4. Real situation examples

For two real situations the statistics for the derived variables and for the basic variables are presented and discussed. The *Geostationary Operational Environment*

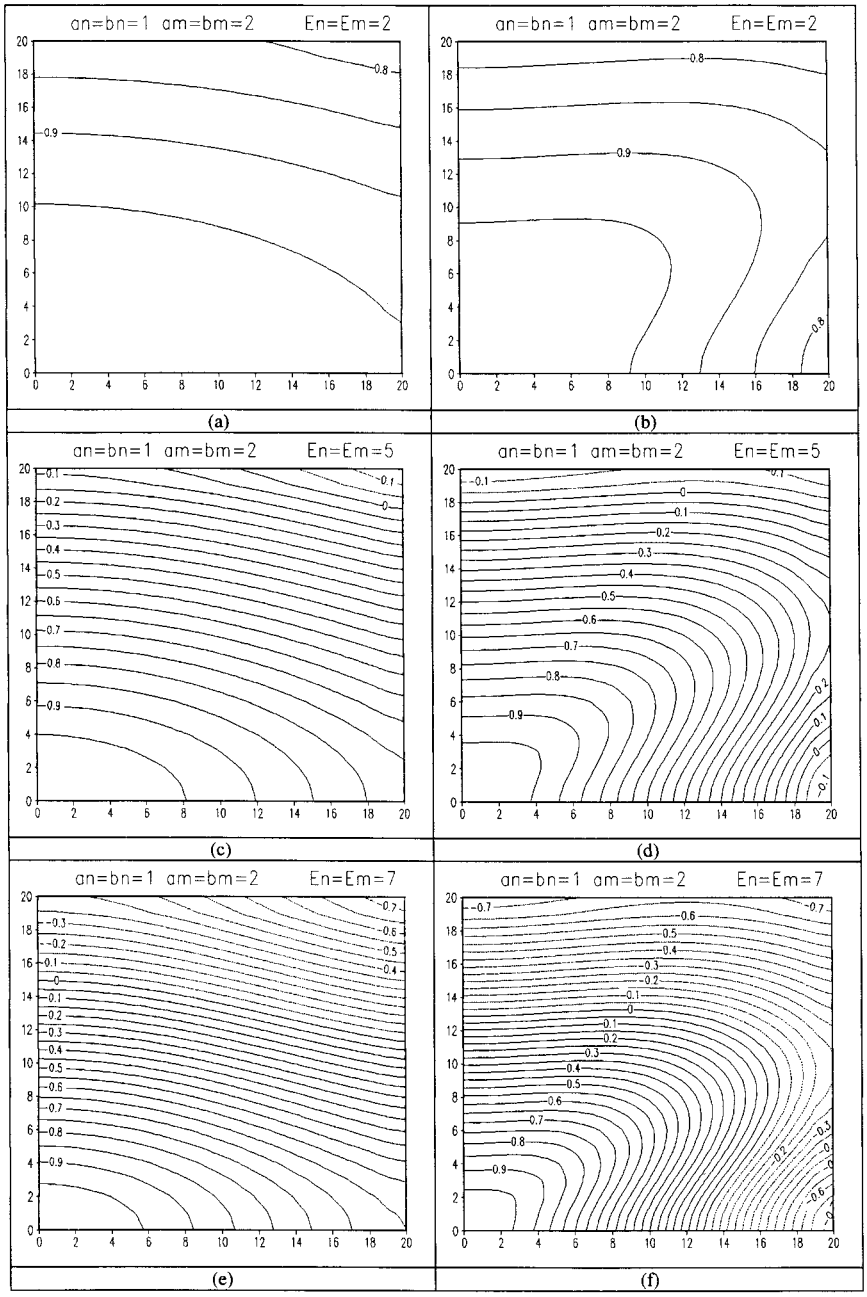

FIG. 4. Same as in Fig. 1 except for $a_n = b_n = 1$ and $a_m = b_m = 2$: (a) $r(F, A)$ for $\epsilon_m = \epsilon_n = 2°$, (b) $r(F_\lambda, A_\lambda)$ for $\epsilon_m = \epsilon_n = 2°$, (c) $r(F, A)$ for $\epsilon_m = \epsilon_n = 5°$, (d) $r(F_\lambda, A_\lambda)$ for $\epsilon_m = \epsilon_n = 5°$, (e) $r(F, A)$ for $\epsilon_m = \epsilon_n = 7°$, (f) $r(F_\lambda, A_\lambda)$ for $\epsilon_m = \epsilon_n = 7°$.

Satellite-8 (*GOES-8*) cloud imagery and the corresponding surface pressure analysis for the synoptic situation of a frontal passage from southeastern Brazil to the South Atlantic during the period 2–4 June 1996 (hereafter referred to as case 1) are shown in Figs. 5 and 6, respectively. In this period the high pressure cell over central parts of South America moved to the Atlantic in the wake of a cold front. A shortwave inverted trough (trough in the easterlies) has intensified in the northern sector of the high pressure cell. Figures 7 and 8 show the cloud imagery and the surface pressure field for the period 26–28 May 1996 during which a shortwave cyclone formed in the South Atlantic near the coast of southern Brazil (hereafter referred to as case 2). The intensification of an inverted trough in the equatorward sector of the high pressure cell into a closed low in the Atlantic off the Uruguay coast is observed in this case. These two examples represent frequently occurring sit-

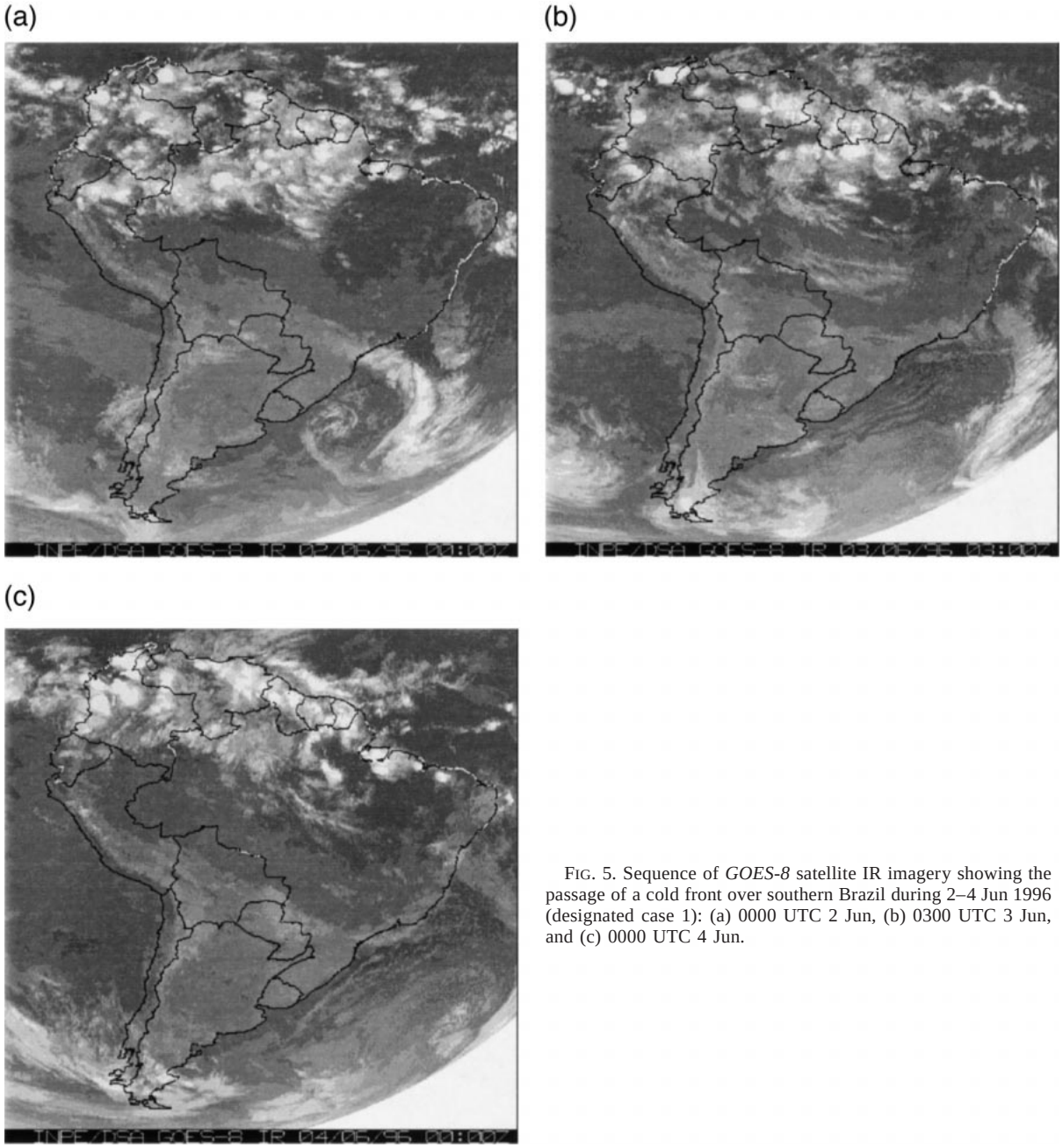

FIG. 5. Sequence of *GOES-8* satellite IR imagery showing the passage of a cold front over southern Brazil during 2–4 Jun 1996 (designated case 1): (a) 0000 UTC 2 Jun, (b) 0300 UTC 3 Jun, and (c) 0000 UTC 4 Jun.

uations in which synoptic systems of extratropical origin are responsible for active weather over the southern half of Brazil in early winter. They cause freezes in the southern and southcentral states of Brazil that are responsible for highly feared damages to the agriculture sector.

The performance statistics at intervals of 24 h up to the forecast range of 6 days are shown in Figs. 9 and 10 for two cases: frontal passage and cyclogenesis, respectively. Each panel of the figures contain three curves, one each for the spatial anomaly correlation coefficient (CC), the spatial standard deviation normalized with the standard deviation of the initial field (SDN), and the root-mean-square error of the forecasts with respect to the verifying analysis normalized with the standard deviation of the initial state (RMSN). The numerical values of the initial spatial standard deviation used for the normalization of the SDN and RMSN are shown on top of each panel. The values shown by the curves are the mean values for the three NWP runs valid for 0000 UTC of the three days of the synoptic episode. That is, the statistics obtained for 2, 3, and 4 June 1996 are averaged and presented in Fig. 9. Similarly the statistics obtained

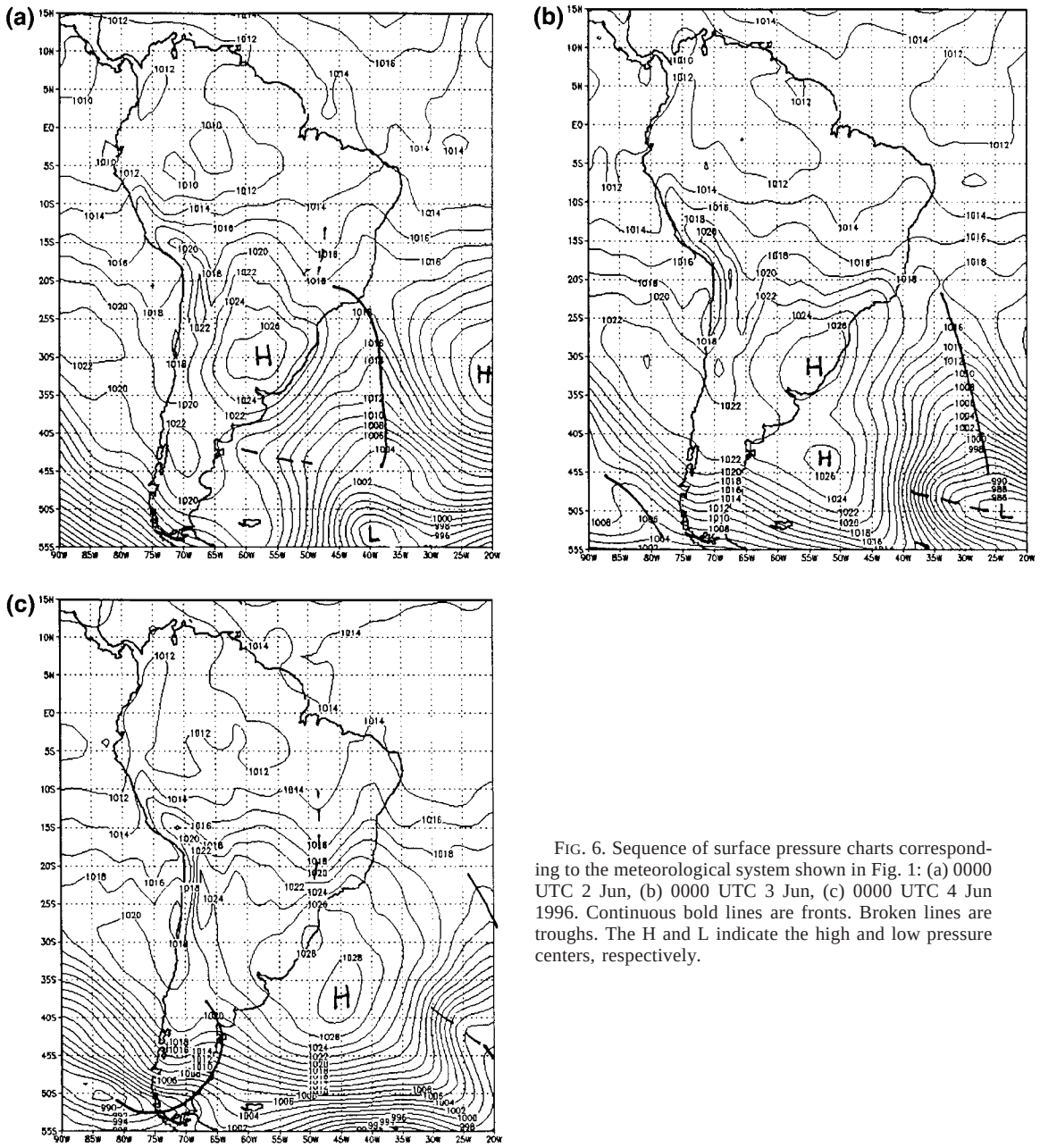

FIG. 6. Sequence of surface pressure charts corresponding to the meteorological system shown in Fig. 1: (a) 0000 UTC 2 Jun, (b) 0000 UTC 3 Jun, (c) 0000 UTC 4 Jun 1996. Continuous bold lines are fronts. Broken lines are troughs. The H and L indicate the high and low pressure centers, respectively.

for 26, 27, and 28 May 1996 are averaged and presented in Fig. 10. In this study the range of useful forecasts (RUF) is considered to be the time at which the anomaly correlation curve intersects the 60% line.

The figures show, in general, that the root-mean-square error of the forecasts with respect to the observed analysis (RMSN) increases first rapidly and then slowly while the anomaly correlation (CC) falls first gradually and then rapidly, with the forecast range. The error grows more rapidly in the lower troposphere than in the middle and upper troposphere. The error almost never has surpassed the standard deviation in the first 5 to 6 days for the basic wind fields, while for the derived fields it has grown larger than SDN within 3 days. The SDN (which expresses the spatial variance of the variable) varies only within 25% of the initial values, in general, decreasing for the first 3 days and then increasing in the next 3 days of the forecast range. The RMSN values are seen to be better behaved than the CC values and it is profitable to consider RMSN $= 1.0 - 1.0/e \approx$ 0.64 as a reasonable limit for the error saturation. In Fig. 9 error saturates roughly at 3 days for u_{500} and v_{500}, whereas it saturates rapidly within 2 days for vorticity and 1 day for vorticity advection.

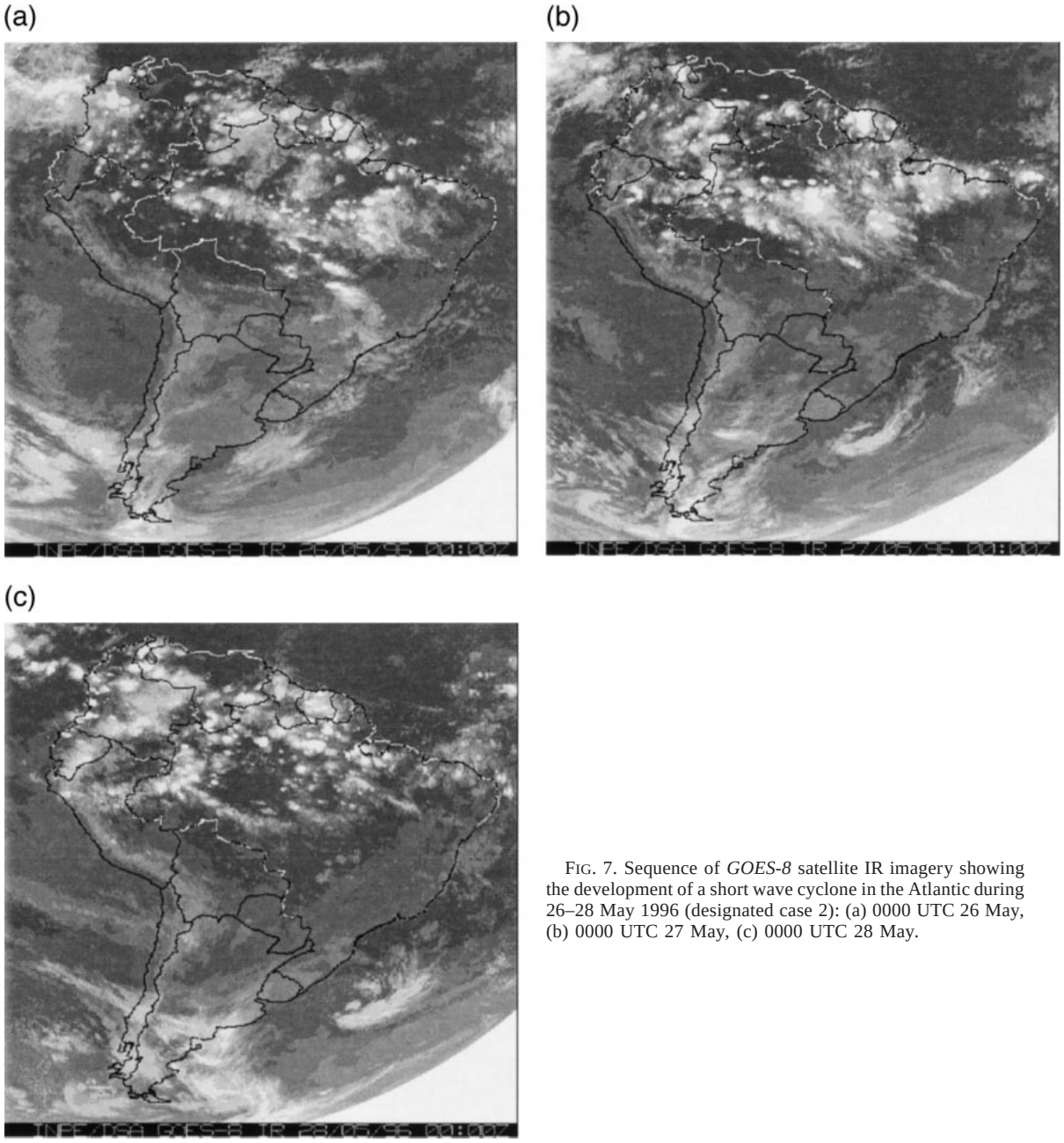

FIG. 7. Sequence of *GOES-8* satellite IR imagery showing the development of a short wave cyclone in the Atlantic during 26–28 May 1996 (designated case 2): (a) 0000 UTC 26 May, (b) 0000 UTC 27 May, (c) 0000 UTC 28 May.

For the frontal passage episode the RUF for the upper-level winds is about 4–5 days and is substantially larger than in the lower troposphere. The RUF for u is more than for v in the upper levels (500 and 200 hPa). The opposite is true in the lower troposphere (850 hPa). The specific humidity and the virtual temperature in the 850-hPa level also have RUFs of 4 days. But, when it comes to the derived fields, the divergence and the convergence of humidity flux (Figs. 10m and 10o), the RUFs are very small with values of a day or less. The thermal advection field in the lower levels demonstrates a RUF of 3 days. This indicates that the forecasts of the frontal passage should be useful for 48- and 72-h lead times; however, the rainfall that accompanies the front is difficult to predict, because the lower-tropospheric humidity convergence determines the precipitation, to a large extent. The 500-hPa vorticity field, which is the first derivative of the flow field, has a RUF of only 60 h, and the vorticity advection that is a product of the wind and the first derivative of the vorticity field has a RUF of just over 1 day. The standard deviation of v falls more rapidly than that of u, and perhaps a large part of the vorticity is in the v component and hence

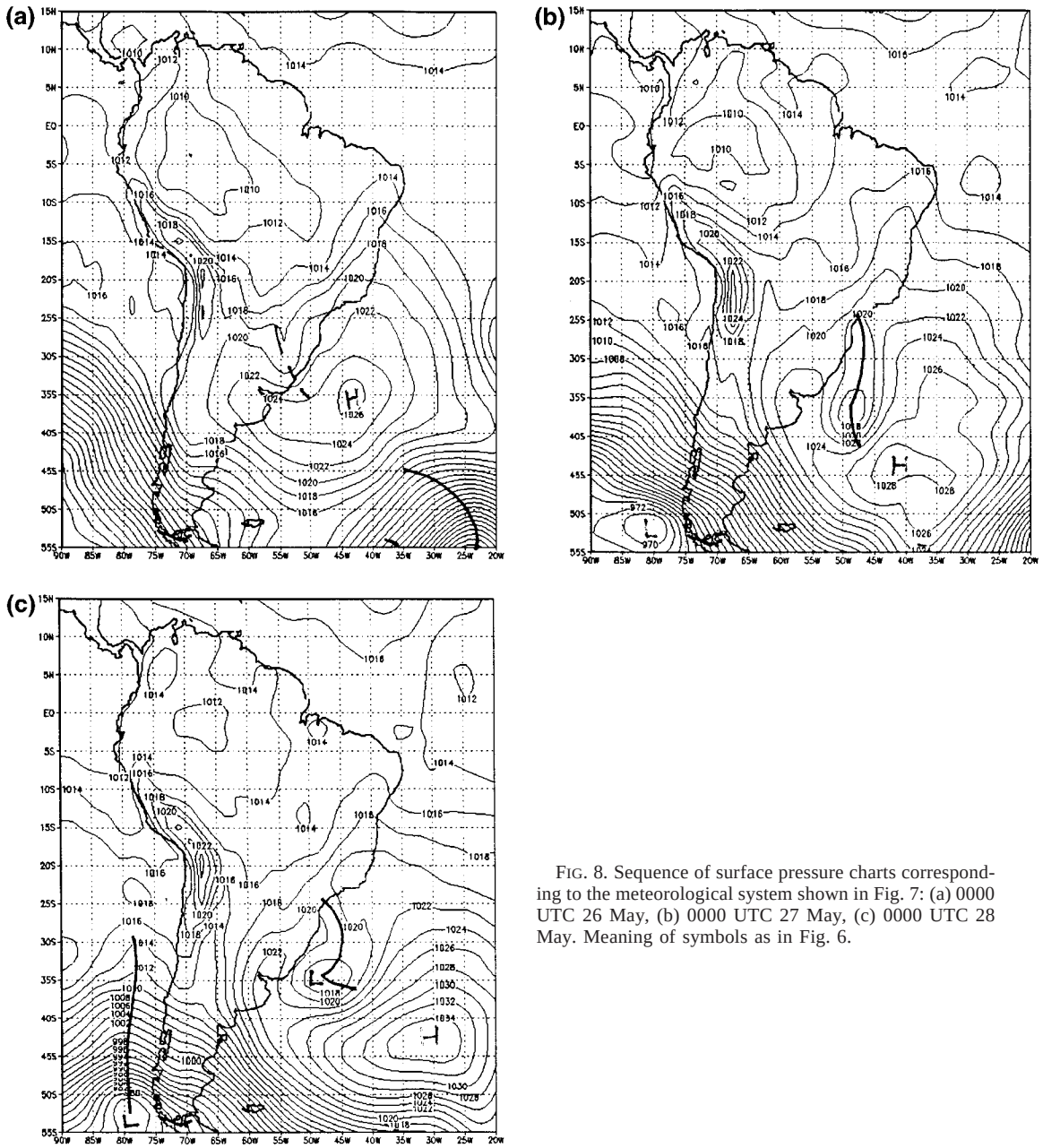

FIG. 8. Sequence of surface pressure charts corresponding to the meteorological system shown in Fig. 7: (a) 0000 UTC 26 May, (b) 0000 UTC 27 May, (c) 0000 UTC 28 May. Meaning of symbols as in Fig. 6.

the performance of the forecast of vorticity and its advection decrease. The RUF of the vorticity field is larger at the 200-hPa level than at the 500-hPa level. This can be understood by noting that the vorticity in the upper troposphere is largely due to the meridional variation of the zonal flow, which has a larger RUF than the meridional wind. The subtropical jet and its gradual northward migration along with the frontal system in the South American region, whose forecast shows good performance in terms of the temperature and related fields, contribute to better performance of the vorticity and its advection at 200 hPa.

In the case of the short wave cyclone development in the South Atlantic the results are quite similar to those in the frontal passage case. However, some minor but interesting differences are worth noting. The error in the humidity flux convergence is more than 50% larger than the initial standard deviation even at a lead time of 24 h and it grows further afterward. (This is the reason for Fig. 10o not having the RMSN curve.) The error in the wind component forecasts almost never surpasses the spatial standard deviation in this case. However, the vorticity advection in the middle and upper troposphere have very low RUF (about 1 day)

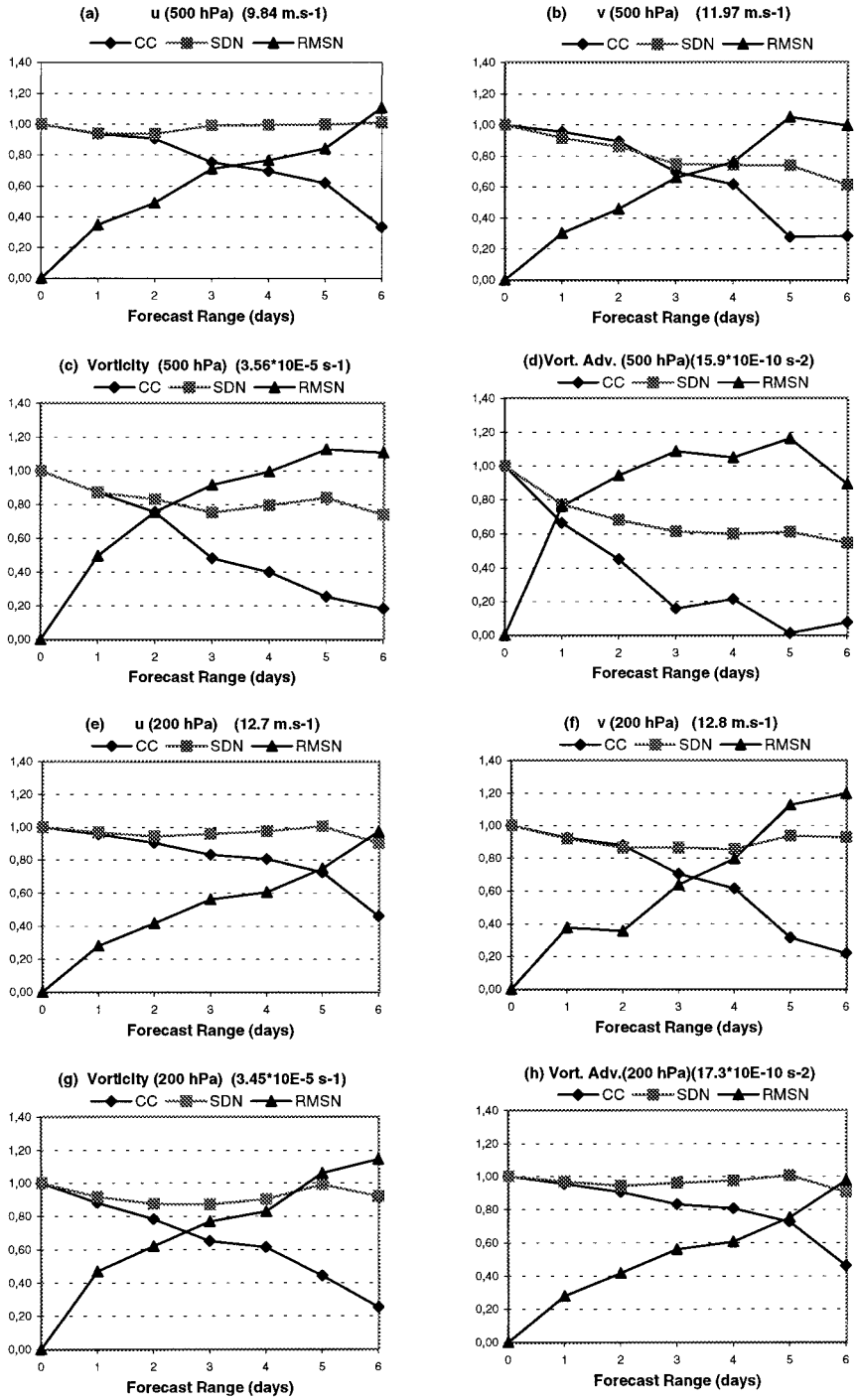

FIG. 9. Average model performance statistics for the case of frontal passage (case 1). Meteorological variable and level are shown on individual panels (a)–(o). Here, *u* and *v* are zonal and meridional components of wind, TV is virtual temperature, SH is specific humidity, DIV is divergence, ADVT is thermal advection, CONV Q is humidity flux convergence. Each panel

compared to the earlier case (more than 3 days). This is very likely due to difference in the phase of the short wave in the forecast with respect to the verifying analysis.

5. Summary and conclusions

The performance statistics of numerical weather prediction models applied to derived atmospheric fields

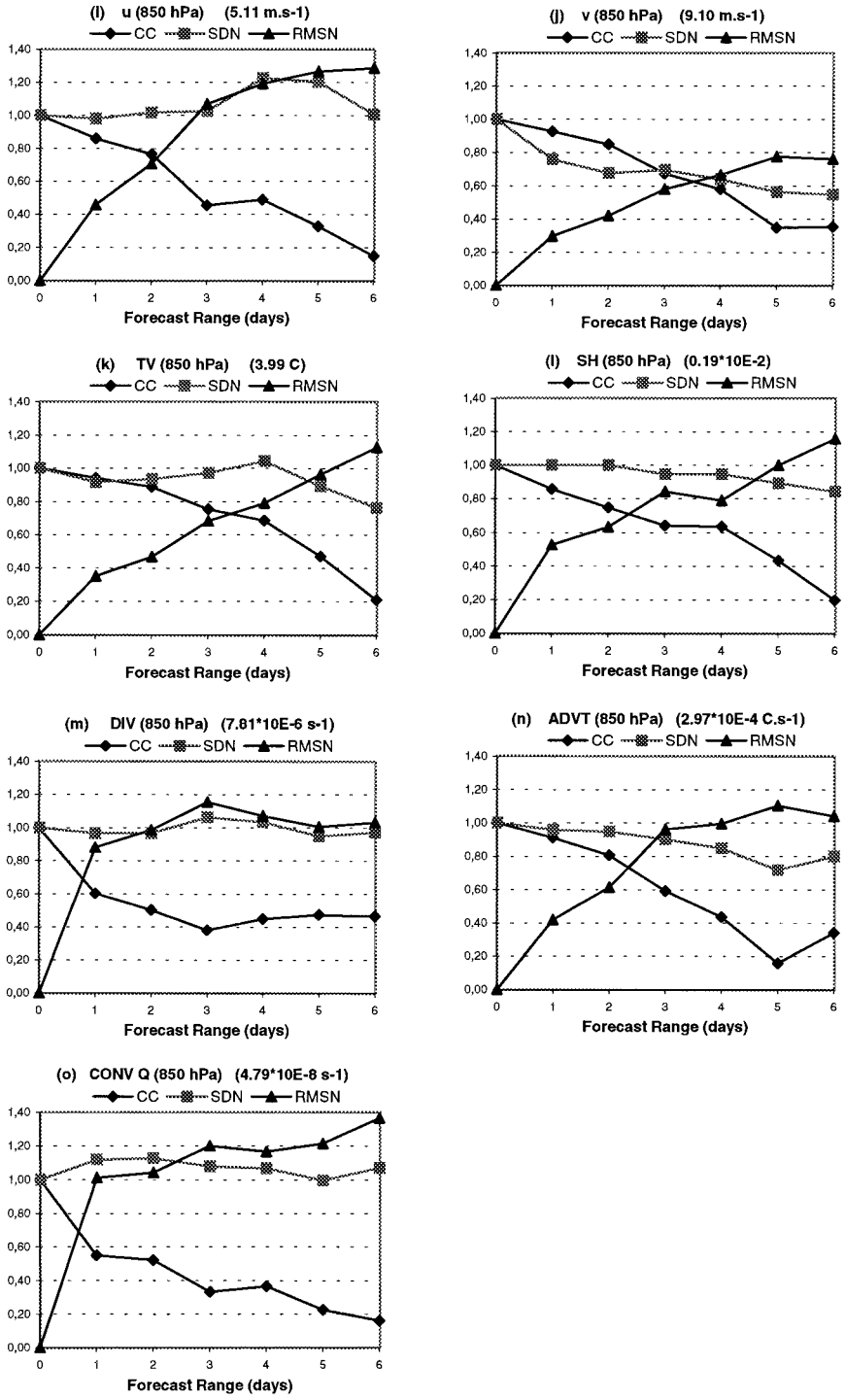

FIG. 9. (*Continued*) contains three curves: anomaly correlation (CC), normalized spacial standard deviation (SDN), and normalized root-mean-square error (RMSN). Numerical values of the initial spatial standard deviation used for normalization of the SDN and RMSN curves are shown at the top of each panel.

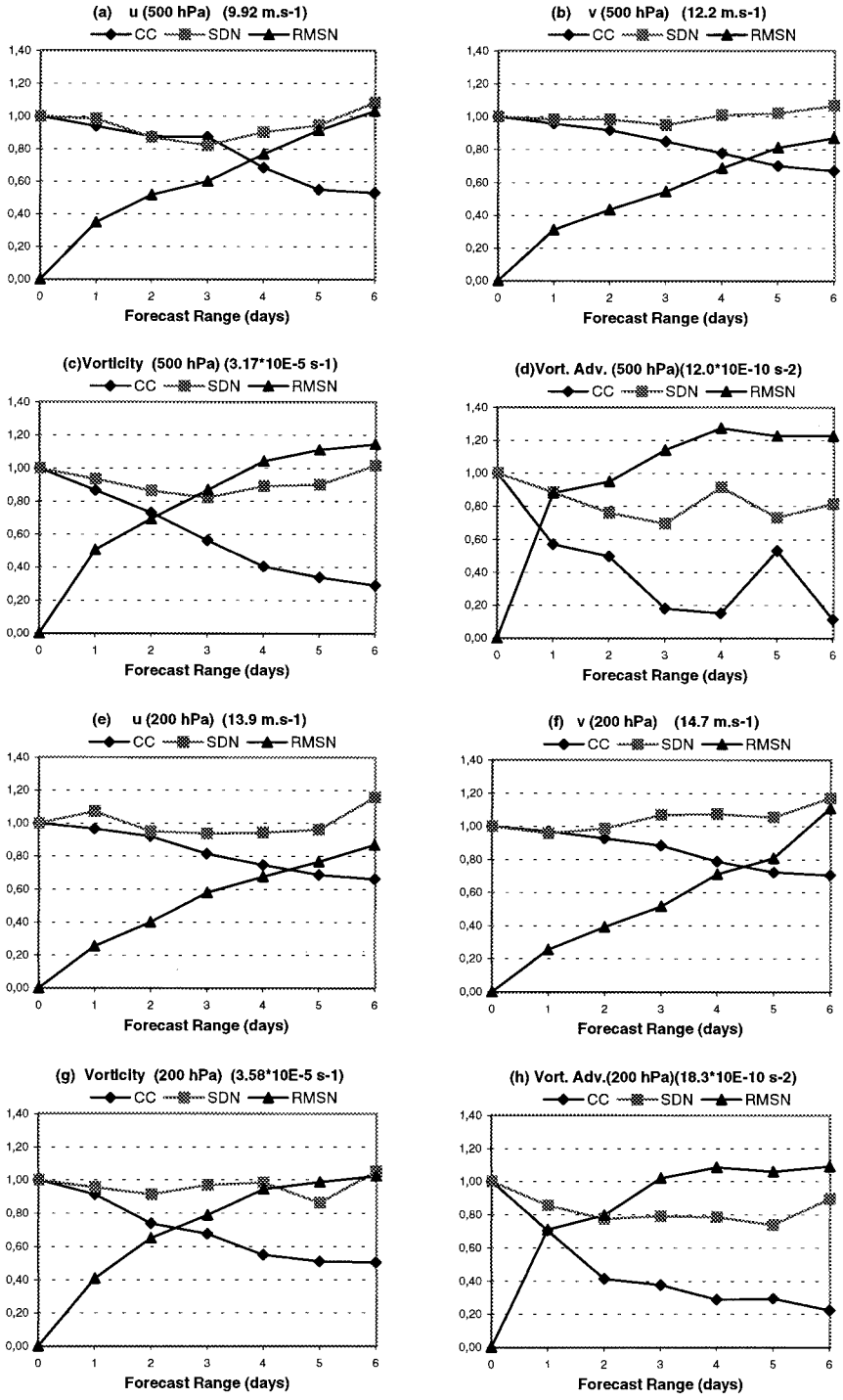

FIG. 10. Same as in Fig. 9 except for the case of development of a low (case 2).

such as humidity convergence or thermal advection can be quite different from those applied to simple or basic model output variables such as wind components or temperature. The prediction skill as estimated from the anomaly correlation and root-mean-square error with respect to the observed fields depends heavily on the phase of the shortwave components of the synoptic situation.

A simple analysis with a combination of two harmonics m and n in one dimension (λ) shows large differences between the correlations for the basic fields and the correlations for the derived fields. Shortwave

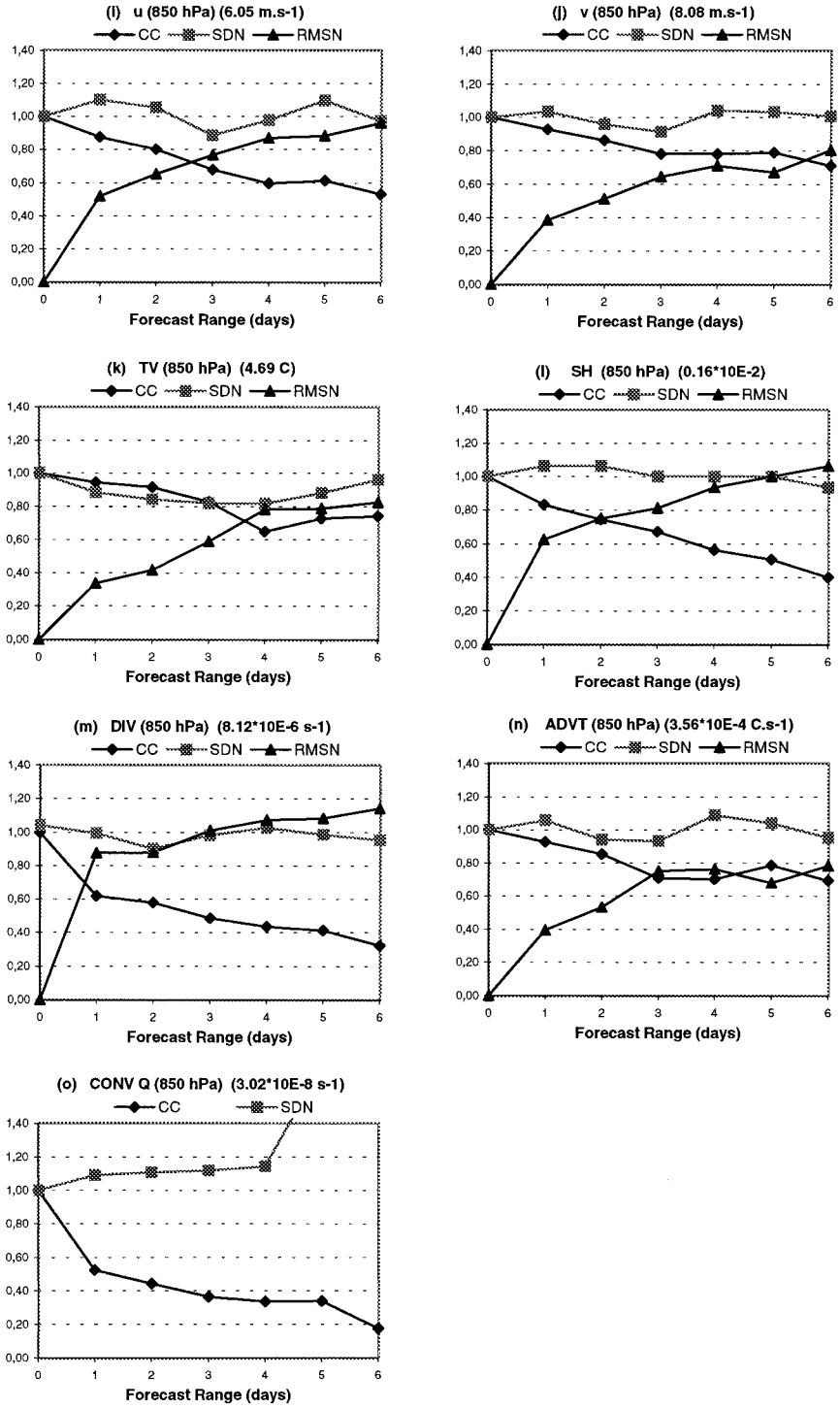

FIG. 10. (*Continued*)

phase forecast errors make the correlation for the derived fields significantly different from those for the basic fields. For a reasonable value of 2° for the phase error of the shortwave component the correlation for the derived fields can be less than 0.5 while the correlation for the basic fields is as high as 0.9. Interesting characteristics of the dependency of the correlation on the wavenumbers and their phase errors can be seen in Figs. 1–4.

The CPTEC–COLA NWP operational model performance in terms of derived fields over the South American region is obtained and is compared to the perfor-

mance for simple model output variables. With the aid of two cases of real situations, the prediction skill in terms of derived variables is shown to rapidly dwindle beyond 1–2-days forecast range, although the basic variable statistics show useful skill beyond 72 and 96 h. Interesting synoptic situations contain more variance in short waves and even small errors in the prediction of their phase can drastically reduce the useful length of forecast range in such situations. In the real case of the development of a short wave in the Atlantic the upper-tropospheric vorticity advection performance is very poor, most likely due to the error in the phase of that wave.

A general assumption is that the errors in the forecasts are larger than in the observed fields for the lower-order fields (or basic variable fields) such as geopotential. However, over data-sparse regions the errors in the analysis may be comparable or larger than the errors in the forecasts, especially at short range (up to 2 days). This problem becomes more pronounced for fields like humidity and for the higher-order variables. Thus the error in the moisture convergence satuarates at the very first day of forecast over South America. Therefore the quantitave validity of the statistical results presented here cannot be accepted at face value. This is not due to an inherent lack of predictability nor due to the deficiency in the forecast model. It has to be borne in mind that higher-order fields like moisture convergence cannot be usefully employed in routine weather forecasting activity.

Verification statistics of basic fields such as geopotential and wind components overestimate the skill and usefulness of the forecasts in comparison to those of the derived or higher-order fields that are meteorologically relevant. Inclusion of performance statistics applied to forecast-derived fields such as thermal advection and vorticity advection in the middle and high latitudes and humidity convergence and precipitable water in the Tropics for the intercomparison purposes is recommended.

Acknowledgments. Mr. José Alexandre da Costa Galvão and Mr. Luiz Gustavo G. de Gonçalves helped in the preparation of the figures and Dr. José Paulo Bonatti critically went through the manuscript.

REFERENCES

Bonatti, J. P., 1996: Verificação estatística do modelo global do CPTEC. (Statistical verification of CPTEC global model.) *Proc. IX Brazilian Meteorology Congress,* Campos de Jordão, Sao Paulo, Brazil, 1453–1456. [Available from Sociedade Brasileira de Meteorologia, Departamento de Meteorologia, Universidade Federal de Rio de Janeiro, CEP12-630-000 Rio de Janeiro, Brazil.]

Chen, W. Y., and H. M. Van den Dool, 1995: Forecast skill and low frequency variability in NMC DERF90 experiments. *Mon. Wea. Rev.,* **123,** 2491–2514.

Harshvardhan, R. Davies, D. A. Randall, and T. G. Corsetti, 1987: A fast radiation parameterization for general circulation models. *J. Geophys. Res.,* **92,** 1009–1016.

Kirtman, B., A. Vemekar, D. DeWitt, and J. Zhou, 1993: Impact of orographic gravity wave drag on extended-range forecasts with the COLA GCM. *Atmosfera,* **6,** 3–23.

Lacis, A. A., and J. E. Hansen, 1974: A parameterization for the absorption of solar radiation in the earth's atmosphere. *J. Atmos. Sci.,* **31,** 118–133.

Mellor, G. L., and T. Yamada, 1982: Development of turbulence closure model for geophysical fluid problems. *Rev. Geophys. Space Phys.,* **20,** 851–875.

Miyakoda, K., and J. Sirutis, 1986: *Manual of the E-physics.* Princeton University, 122 pp. [Available from Geophysical Fluid Dynamics Laboratory, Princeton University, P.O. Box 308, Princeton, NJ 08542.]

Sela, J., 1980: Spectral modeling at the National Meteorological Center. *Mon. Wea. Rev.,* **108,** 1279–1292.

Sellers, P. J., Y. Mintz, Y. C. Sud, and A. Dalcher, 1986: A simple biosphere model (SiB) for use within general circulation models. *J. Atmos. Sci.,* **43,** 505–531.

Slingo, J. M., 1987: The development and verification of a cloud prediction model for the ECMWF model. *Quart. J. Roy. Meteor. Soc.,* **113,** 899–927.

Stanski, H., L. J. Wilson, and W. R. Burrows, 1990: A survey of common verification methods in meteorology. WWW Tech. Rep. 8, World Meteorological Organization, 113 pp.

Tiedtke, M., 1983: The sensitivity of the time-mean large-scale flow to cumulus convection in the ECMWF model. *Proc. ECMWF Workshop on Convection in Large-Scale Models,* Reading, United Kingdom, European Centre for Medium-Range Weather Forecasts, 297–316.

Wilks, D. S., 1995: *Statistical Methods in the Atmospheric Sciences.* Academic Press, 464 pp.

Wobus, R. L., and E. Kalnay, 1995: Three years of operational forecast skill at NMC. *Mon. Wea. Rev.,* **123,** 2132–2148.

Xue, Y.-K., P. J. Sellers, J. L. Kinter III, and J. Shukla, 1991: A simplified biosphere model for global climate studies. *J. Climate,* **4,** 345–364.